Morán-Pedroso, M., Gago, R., Julin, J., Salas-Colera, E., Jimenez, I., de Andrés, A. & Prieto, C. (2021). Correlated effects of fluorine and hydrogen in fluorinated tin oxide (FTO) transparent electrodes deposited by sputtering at room temperature. Applied Surface Science, 537, 147906.

DOI: 10.1016/j.apsusc.2020.147906

Applied Surface Science 537 (2021) 147906

Contents lists available at ScienceDirect

Applied Surface Science

journal homepage: www.elsevier.com/locate/apsusc

Correlated effects of fluorine and hydrogen in fluorinated tin oxide (FTO) transparent electrodes deposited by sputtering at room temperature

María Morán-Pedroso[a], Raúl Gago[a], Jaakko Julin[b,c], Eduardo Salas-Colera[a,d], Ignacio Jimenez[a], Alicia de Andrés[a], Carlos Prieto[a,*]

[a] Instituto de Ciencia de Materiales de Madrid (ICMM), Consejo Superior de Investigaciones Científicas (CSIC), Cantoblanco, 28049 Madrid, Spain
[b] Institute of Ion Beam Physics and Materials Research, Helmholtz-Zentrum Dresden – Rossendorf e.V. (HZDR), Bautzner Landstraße 400, 01328 Dresden, Germany
[c] Department of Physics, University of Jyväskylä, P.O.Box 35, 40014 Jyväskylä, Finland
[d] Departamento de Física, Escuela Politécnica Superior, Universidad Carlos III de Madrid, Avenida Universidad 30, Leganés, 28911 Madrid, Spain

ARTICLE INFO

Keywords:
Transparent conductive materials
Fluorinated tin oxide
Room temperature film preparation

ABSTRACT

The optical and electrical properties of fluorinated tin oxide (FTO) films deposited at room temperature by sputtering have been investigated varying the fluorine content and the hydrogen atmosphere. The complex behavior of the obtained films is disclosed using a wide set of characterization techniques that reveals the combined effects of these two parameters on the generated defects. These defects control the electrical transport (carrier density, mobility and conductivity), the optical properties (band gap and defects-related absorption and photoluminescence) and finally promote the amorphization of the samples. H_2 in the sputtering gas does not modify the H content in the films but induces the partial reduction of tin (from Sn^{4+} to Sn^{2+}) and the consequent generation of oxygen vacancies with shallow energy levels close to the valence band. A variation of up to four orders of magnitude in electrical conductivity is reported in samples with the appropriate fluorine doping and hydrogen fraction in the sputtering gas, maintaining excellent optical transparency. Optimized room temperature grown electrodes reach sheet resistance ~20 Ω/□ and transparency > 90%. This room temperature deposition process enables film preparation on flexible organic substrates, such as polyethylene terephthalate (PET), with identical performance of doubtless interest in flexible and large scale electronics.

1. Introduction

Technologies for photovoltaic energy harvesting and light emitting devices are strongly dependent on the research on new transparent conductive materials (TCM) including its processing and the production methods [1,2]. Typically, high temperature processes are necessary to obtain a TCM with optimized performance [3] however, film preparation at nearly room temperatures is of particular interest for flexible electronics and also for the coating of large area glasses as those used in architectural windows. Indium tin oxide (ITO) is the most commonly used TCM in electronic devices because of its excellent electrical and optical properties [4], but research on indium-free materials has become highly interesting due to indium scarcity and also to further enhance TCM functionality for some specific applications. In this sense, tin oxide based TCMs are excellent materials for transparent electrodes due to the low cost, high stability and adequate mechanical properties.

Fluorinated tin oxide (FTO) is a typical n-type TCM with excellent optical properties (high transmittance and wide band gap) and suitable conductivity. Among other deposition techniques, such as spray pyrolysis or pulsed laser deposition [5–9], sputtering has been used to prepare FTO from different starting materials as metallic Sn [10], blended SnF_2-Sn [11], mixed oxide fluoride SnO_2-SnF_2 [12,13]. Independently of the deposition technique, preparation at nearly room temperature is a requirement for films supported on organic substrates. However, FTO with suitable conductivity is usually obtained by high temperature deposition techniques or with post-deposition annealing processing [14,15]. To circumvent this issue, the use of hydrogen in the sputtering working gas has been demonstrated to be an effective way for ITO preparation at room temperature with improved conductivity without transparency worsening [16,17], as reported for ITO deposited on organic flexible substrates [18]. In this context, the influence of H_2 in the sputtering gas has been studied for FTO preparation at moderately high temperature (300 °C) [15] and room temperature [19].

To enlighten the different processes that contribute to determine the conductivity in FTO, in this paper we report a detailed study on FTO films deposited by sputtering using hydrogen in the sputtering gas. The

* Corresponding author.
E-mail address: cprieto@icmm.csic.es (C. Prieto).

https://doi.org/10.1016/j.apsusc.2020.147906
Received 30 July 2020; Received in revised form 11 September 2020; Accepted 13 September 2020
Available online 16 September 2020
0169-4332/

effect of hydrogen partial pressure on the optical and electrical properties in several FTO series with different fluorine contents is analyzed in parallel with its elemental composition, crystallographic film structure, tin and oxygen local valence bonding and oxygen defects.

2. Experimental

FTO films were deposited on fused silica, polyethylene terephthalate (PET) and Si(1 0 0) substrates by DC magnetron sputtering from 2 in. FTO ceramic targets. Blends of SnO_2 and SnF_2 with weight ratios 94:6 and 80:20 were pressed with 100 Kg/cm^2 to obtain disks of nearly 3 mm in height and then heated to 400 °C during 2 h. Within these conditions, the X-ray diffraction analysis of the as-processed targets show no diffraction peaks from SnF_2, proving that fluorine has entered into the SnO_2 structure. Consequently, the obtained disks are conductive enough to allow DC sputtering.

The sputtering chamber had a typical base pressure of 1×10^{-4} Pa and a load-lock attached chamber was used for introducing the substrate. After pre-sputtering target cleaning, the film deposition process was carried out with different Ar, H_2 and O_2 gas mixtures at constant pressure of 0.65 Pa with variable $H_2/(H_2 + O_2 + Ar)$ content from 0 to 1% and constant $O_2/(H_2 + O_2 + Ar)$ content of 5%. Gas flows are regulated by three independent mass flow controllers (from Bronkhorst). Typically, FTO films of 300 nm thickness were obtained with deposition rates of 5 nm/min by using DC power of 20 W.

The room temperature electrical properties were obtained with a Keithley 2400 source-meter and a Keithley 2000 digital voltmeter managed by home-made computer software to quantify I-V and V-H curves. According with the van der Pauw method [20,21], four silver paint contacts were placed on the FTO films surface corners of squared samples to measure its sheet resistance (R_S). Hall effect measurements were made at room temperature by placing samples in a variable magnetic field provided by a standard electromagnet (-0.8 T $< H <$ 0.8 T). Resistivity (ρ), charge carrier density (N) and optical absorption coefficient (α) were calculated after measuring the films thickness with a Veeco Dektak 150 profilometer.

The optical transmission characterization was performed by using a Cary-4000 Varian spectrophotometer in the 200–900 nm wavelength range. The signal from the substrate was eliminated by measuring the corresponding bare substrates. The samples were also analyzed by spectroscopic ellipsometry (SE) with a GES-5E (SOPRA©) ellipsometer within the 1.5–5 eV spectral range. A Tauc-Lorentz (TL) optical model was used for data fitting to extract the optical constants. It should be noted that the TL description is normally suitable for amorphous or nanocrystalline semiconductors and dielectrics [22]. Raman and photoluminescence (PL) experiments were performed at room temperature with the 488 nm line of an Ar^+ laser, incident power of 10 mW, an Olympus microscope, and a "super-notch-plus" filter from Kaiser. The scattered light was analyzed with a Jobin-Yvon iHR-320 monochromator coupled to a Peltier cooled Synapse CCD (charge-coupled device).

Rutherford backscattering spectrometry (RBS) was performed at the 5 MV HVEE Tandetron accelerator located at the Centro de Micro-Análisis de Materiales of the Universidad Autónoma de Madrid [23]. RBS experiments were performed with helium ions of energy close to 2 MeV. Compositional characterization of the films, including light elements such as H, was carried out by means of heavy-ion elastic recoil detection analysis (ERDA). The measurements were performed with 35 MeV Cl^{7+} projectiles impinging at an incidence angle of 75° with respect to the sample surface normal. The scattered projectiles and recoiled sample atoms were detected with a Bragg ionization chamber positioned at a scattering angle of 31°, allowing the discrimination of detected particles according to their atomic number. The analysis of the recoil spectra and scattered Cl spectrum was performed simultaneously for each sample with the NDF code [24].

The electronic structure was studied with X-ray absorption near-edge structure (XANES). This technique provides information of electronic states for each individual element, being a powerful technique to study complex multi-element systems. XANES measurements were carried out at the dipole beamline PM3 of the synchrotron facility BESSY-II of Helmholtz-Zentrum Berlin (HZB).

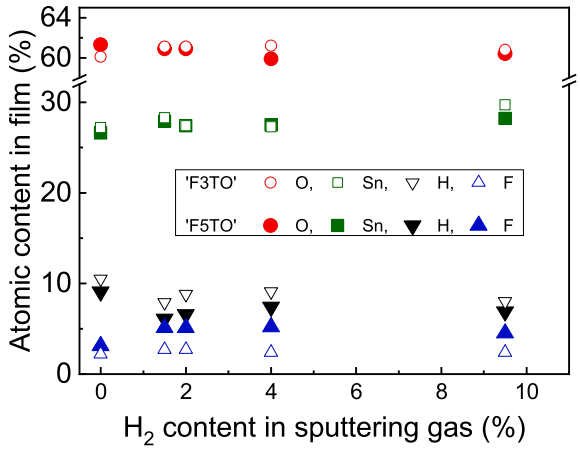

Fig. 1. Atomic composition 'F3TO' and 'F5TO' series vs. the H_2 concentration in the sputtering gas.

3. Results

3.1. Compositional characterization

Element composition of FTO films was checked by RBS and ERDA to determine the actual content of fluorine and hydrogen in several series of samples deposited from SnO_2-SnF_2 cathodes with different SnF_2 concentrations and different H_2 content in the sputtering gas [25]. According with the fluorine content obtained by RBS and/or ERDA, the four FTO studied series will be referred to as 'F1.5TO', 'F3TO', 'F5TO' and 'F8TO' so that 1.5, 3, 5 and 8 indicate the F at% content in the films.

ERDA allows measuring the hydrogen amount across the thickness of the films. It shows that Sn, O, F and H are homogeneously distributed in depth. Fig. 1 shows ERDA outcomes corresponding to 'F3TO' and 'F5TO' series. The results show no clear trend of the hydrogen amount in the films as a function of H_2 content in the sputtering gas. In fact, samples produced with no H_2 in the gas discharge present a relatively higher H content in the films, which may be related with residual water in the base pressure. Nevertheless, hydrogen content is higher in the series with less fluorine ('F3TO') compared to that with more fluorine ('F5TO'), suggesting a correlated effect between both foreign ions (H and F). Regardless of whether hydrogen is present in an atomic form or molecularly occluded in the films, the average chemical formulae obtained by ERDA for the 'F3TO' and 'F5TO' series are $Sn_{0.92}O_2F_{0.08}H_{0.28}$ and $Sn_{0.90}O_2F_{0.15}H_{0.23}$, respectively. Fluorine contents of 2.7% and 4.9% are obtained, which justify the labelling (3 and 5) of the series.

3.2. Conductive properties

Recently, we reported [19] on the interesting electrical behavior of FTO with high fluorine content, 'F8TO' series, that we include here together with the series with lower fluorine content to contribute to an ampler understanding of the FTO system. Fig. 2(a) shows the resistivity of all the studied series.

A clear decrease of resistivity (two orders of magnitude) upon F-doping is observed without H_2 in the sputtering gas, saturating at around 5 at.% F. Regarding the effect of H_2, fluorine free tin oxide samples show no significant change in their properties. However, low fluorine content series ('F1.5TO', 'F3TO' and 'F5TO') show a

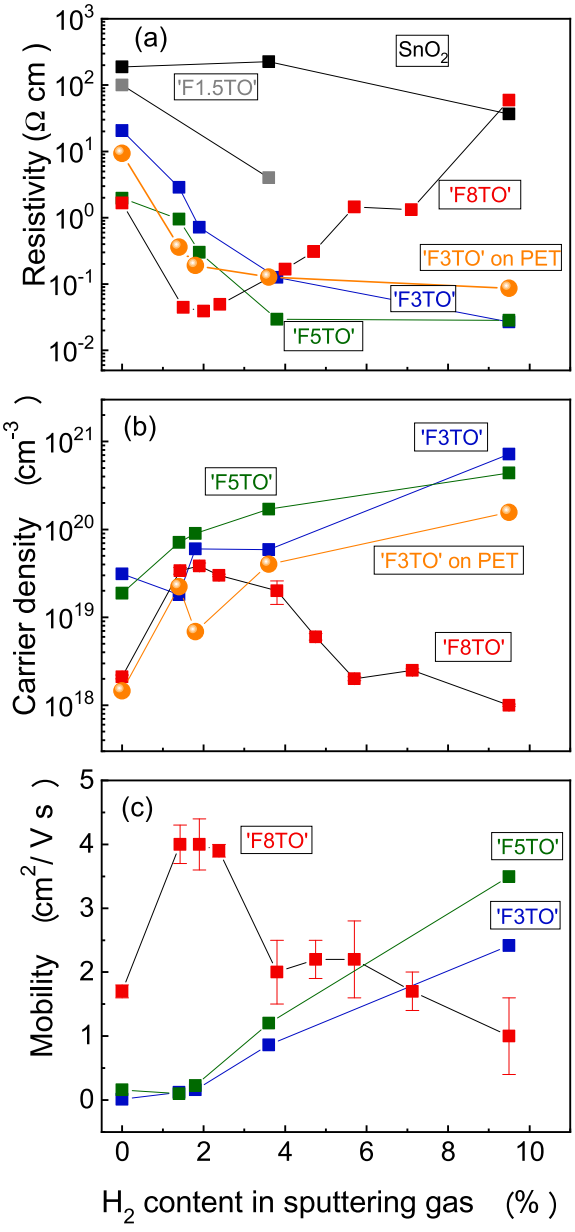

Fig. 2. Electrical characterization of samples series. (a) Resistivity; (b) Charge carrier density; (c) charge Mobility.

monotonous decrease in resistivity with H_2 concentration in the sputtering gas, reaching values close to 10^{-2} Ω cm. Conversely, in the same studied hydrogen range, 'F8TO' series shows a different behavior with a minimum in resistivity. For this 'F8TO' series, very low H_2 concentration (< 2%) in the sputtering gas has a beneficial effect on resistivity, which decreases to near 10^{-2} Ωcm. Nevertheless, for moderate concentrations ($[H_2]$ > 2%), the H_2 effect turns to be detrimental and samples present resistivity values higher than those deposited without H_2. For each fluorine content series, the proper addition of H_2 has a clear beneficial impact on the film electrical properties, inducing a variation over four orders of magnitude in film resistivity.

Fig. 2(b) and (c) show charge carrier density (N) and mobility (μ) for 'F3TO', 'F5TO' and 'F8TO' series with similar behavior as its corresponding conductivity. It is interesting to note that also the 'F8TO' series shows a remarkable enhancement of N and μ in coincidence with the low resistivity regime.

In order to prove the interesting application of room temperature deposition of FTO on organic substrates, we have deposited these series

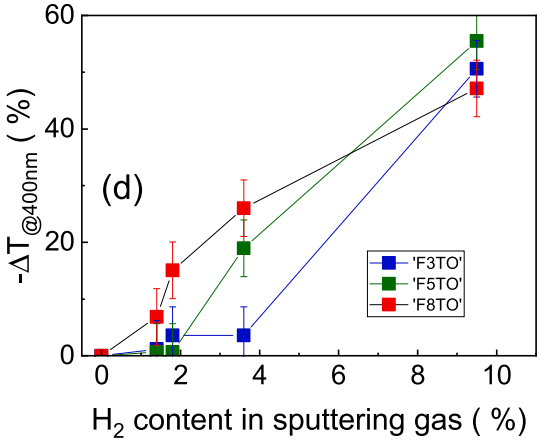

Fig. 3. Variation of the transmittance obtained at 400 nm vs. the hydrogen content in the sputtering gas.

on polyethylene terephthalate (PET) flexible substrates. PET has excellent mechanical properties [26] for polymer solar cells [27] or resistive-type touch screen [28] so that the deposition of TCM films on organic substrates by using low temperature processes is a matter of active research [18,29–31]. Fig. 2 evidences the similar behavior of PET-samples (orange spheres) as those obtained in analogue series deposited on fused silica.

3.3. Optical characterization

Fig. S2 shows optical images of samples from different series deposited on fused silica. All of them are transparent but with different coloring. In Fig. S3, the optical transmission of the three series studied is given. As reported previously [19], H_2 addition induces the presence of a wide absorption band centered near 400 nm, but transparence is not substantially affected at visible wavelengths. Fig. 3 shows the relative decrease of transparence around 400 nm. As discussed below, the higher the fluorine content the lower the H_2 addition is needed to easily observe this broad band.

Band gap energy is typically characterized using the Tauc method [32] by searching the absorption cut-off by extrapolation of a power of the product of the optical absorption (α) measurement near edge multiplied by the photon energy (that is, assuming a behavior near the band-gap onset as $\alpha\, h\nu \sim (h\nu - E_g)^n$, with n ranging from ½ to 2 depending on the optical transition type). There is a large list of methods to evaluate the band gap energy [33] that give similar trends when comparing sample series. For this FTO particular system, the analysis of its gap energy behavior becomes difficult because: (i) the optical absorption at wavelengths near edge is affected by the finite thickness oscillations appearing in thin films (for thicknesses of interest), (ii) the appearance of the broad band around 400 nm in the gap that strongly affects the cut-off extrapolation and (iii) the different degrees of amorphization of the samples. This last point becomes very important because the optical transition type (direct or indirect) may change from crystalline to amorphous samples within the series. For these reasons, we have considered alternatively the optical absorption coefficient raw measurement ($\alpha \sim (h\nu - E_g)$ without any $h\nu$ multiplicand. This procedure gives values in between those obtained considering direct or indirect transitions in the Tauc method. The assumption, that it is not necessary to know the optical transition factor n to determine the gap energy, has already been proposed to overcome unawareness of the transition type [34]. On that way, any mathematical artifacts are avoided to determine gap energy values (E_g) and, what is more interesting, to observe the E_g behavior with H_2 in the studied series. Fig. S4 shows the absorption coefficient of the three relevant series. Firstly, it is interesting to note that, accordingly with the

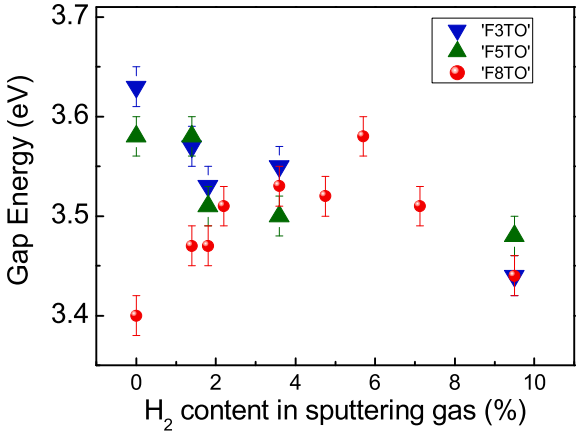

Fig. 4. Band gap energy of the studied FTO series.

reported behavior [35], E_g decreases with fluorine content for the samples grown without H_2 in the gas mixture (see inset of Fig. S4(a)). On the other hand, the E_g behavior as a function of the H_2 content differ for 'F3TO' and 'F5TO' series in comparison to that in 'F8TO' (Fig. 4). Series with small fluorine content present a monotonous E_g decrease with H_2 content in the sputtering gas. However, a fine analysis in 'F8TO' series shows an E_g increase for low H_2 content (< 6%) in sputtering gas followed by a decrease for H_2 content higher than 6%. Fig. 4 summarizes the obtained analysis of E_g values, where it is evidenced that the trends of E_g in the three series behave in some parallel way to resistivity, charge density and mobility (Fig. 2).

Additionally, we have used spectroscopic ellipsometry (SE) to determine the refractive index of FTO samples. Fig. S5 shows the real part of the obtained refractive index and Fig. S6 shows the extinction coefficient of 'F3TO' and 'F8TO' series ('F3TO' and 'F5TO' series have very similar behaviors). Insets of Fig. S5(a) and Fig. S6(a) show a weak variation with fluorine content for the samples grown without H_2 in the gas mixture being an indication of minor contribution of fluorine to optical properties. Conversely, Fig. S5 and Fig. S6 reveal different evolution of refractive index along 'F3TO' and 'F8TO' series, which stand for a stronger influence of H_2 in low fluorine content series ('F3TO' and 'F5TO' series), but very weak in medium fluorine ('F8TO' series) content samples.

3.4. Long-range order characterization

Long-range order was studied by X-ray diffraction (XRD), Fig. 5 shows diffractograms obtained for two FTO series ('F3TO' and 'F5TO'). Measurements indicate a medium-range crystalline order that worsen with increasing H_2 content in the sputtering gas. Moreover, amorphous character is obtained for smaller H_2 content in series with higher fluorine content. In the 'F3TO' series, amorphous films are obtained from 4% H_2 concentration in sputtering gas. A slight change is observed in the 'F5TO' series for which, from only 2% H_2 sputtering gas, the obtained films are mainly amorphous. Moreover, we have not obtained hints of long-range ordering in the 'F8TO' series. This trend points toward the conclusion that H_2 in sputtering gas favors film amorphization that is further facilitated in series with higher fluorine content.

3.5. Local-order bonding characterization

X-ray absorption spectroscopy (XAS) has been used to study the electronic state of tin and oxygen in 'F3TO' and 'F5TO' series. Fig. 6 shows the Sn M_V-M_{IV}- and O K-absorption near edge spectra of samples from 'F5TO' series. The spectral lineshape, for both edges, is rather similar for all the samples except for the higher H_2 case (very similar results are obtained in 'F3TO' series showed in Fig. S6).

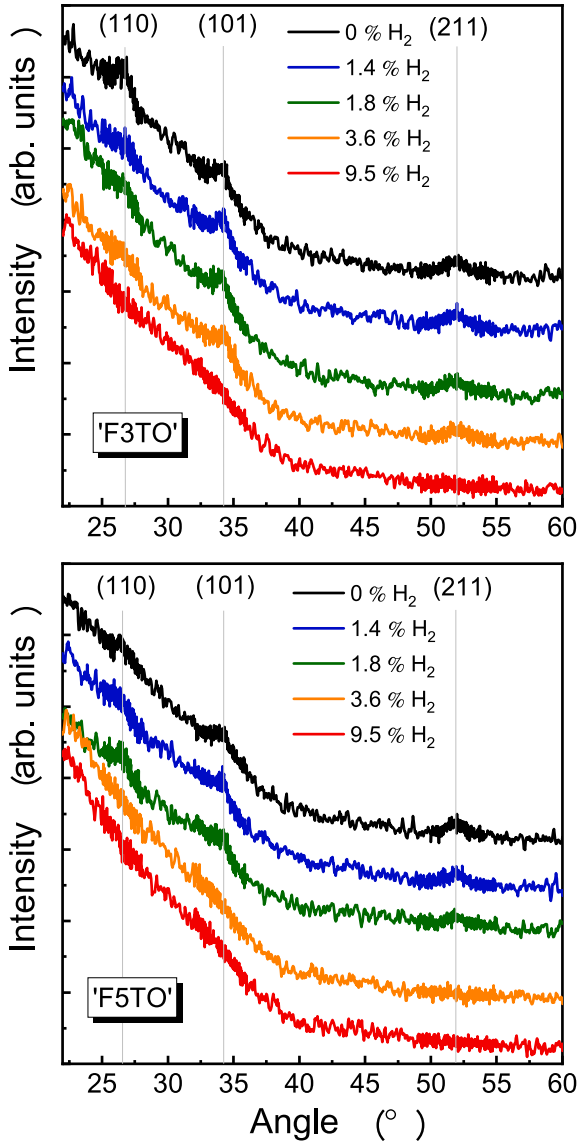

Fig. 5. X-ray diffractograms: (a) 'F3TO' series; (b) 'F8TO' series.

The peak observed in the low energy region of the O K-edge corresponds to the transition from the O 1s core level into primarily O 2p-Sn 5s hybridized a_g states, which forms the bottom of the conduction band (CB) and the features at higher energies corresponds to transitions to O 2p-Sn 5p states (b_{1u}, b_{2u}, and b_{3u}) [36,37]. As observed in tin oxide thin films prepared by the atomic layer deposition technique [38], the low energy peak (at ~537 eV) compared with the feature at higher energies (around ~543 eV) has small changes in their relative intensity and position. The relative increase of a_g intensity in the sample prepared with 9.5% H_2 indicates a higher promotion of transitions to the unoccupied states in the bottom of CB and, on the other hand, the slight decrease of energy implies a slight CB expansion that would increase carrier transport in terms of an extension of the unoccupied conduction band. This effect has been associated with charge mobility increase [39] because of the easier carrier transport to the CB due to the increase in probability of carrier hopping.

On the other hand, the energy onset of the Sn $M_V - M_{IV}$ absorption edges is coincident with SnO_2, showing Sn mainly in 4+ oxidation state; nevertheless, very small variations are detected along the series. The difference between the position of the first peak of oxygen and tin M_V edge may be used to detect small variations in tin oxidation state [40] in the sense that the lower difference in energy values the higher

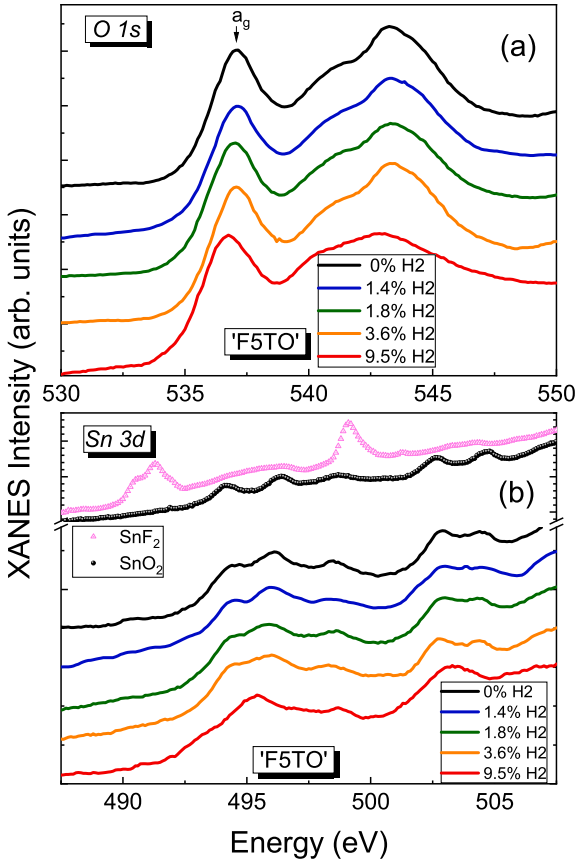

Fig. 6. X-ray absorption near edge spectra of 'F5TO' samples: (a) oxygen 1s absorption edge; (b) tin 3d absorption edges (includes comparison with tin fluoride and tin oxide).

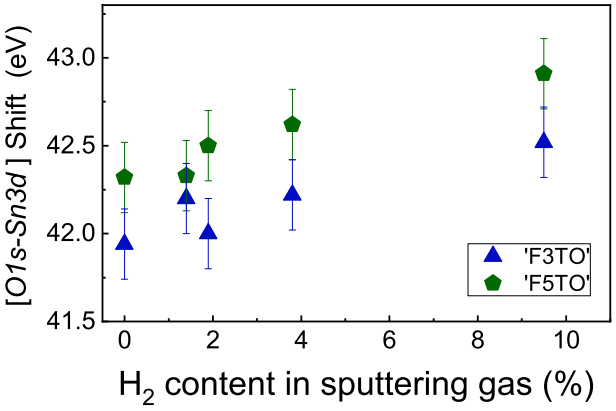

Fig. 7. Evolution of the energy difference between the tin 3d and the oxygen 1s absorption edges (evaluated at the main jump).

oxidation state. Fig. 7 shows a small, but measurable and systematic, increase of the *O 1s* to *Sn 3d* energy difference with the H_2 content in the sputtering gas revealing a continuous decrease of Sn oxidation state (from the +4 nominal state) in both 'F3TO' and 'F5TO' series. Assuming a linear behavior of Sn oxidation state change vs. the *O 1s* to *Sn 3d* energy difference, a reduction of ~0.3 units in the average oxidation state of Sn can be estimated along each series, resulting in ~15% Sn^{2+} increase. Another interesting point is that, for samples made with the same H_2 amount; 'F5TO' presents lower average Sn oxidation than 'F3TO' series. This comparison between series estimates an average tin reduction of ~0.16 units, resulting in ~8% Sn^{2+} increase due to the increased amount of fluorine in 'F5TO' compared to 'F3TO'.

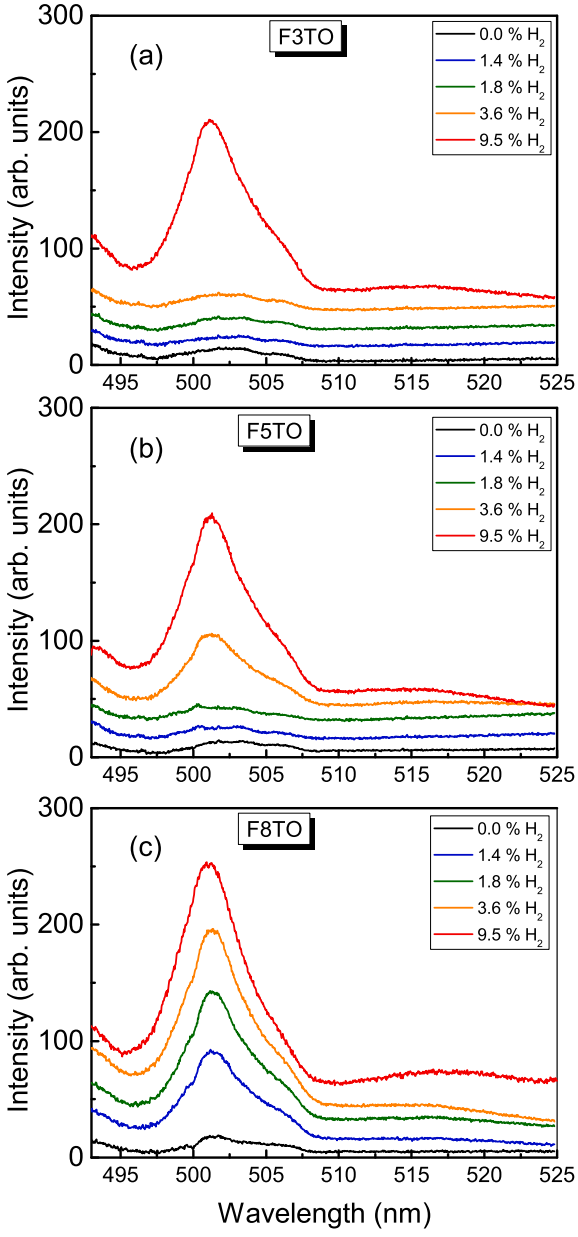

Fig. 8. Evolution of photoluminescence in studied series. (a) 'F3TO' series, (b) 'F5TO' series, (c) 'F8TO' series.

3.6. Defect structure characterization

The photoluminescence (PL) associated to defects in SnO_2 has been extensively studied [41–44] but the exact origin of the observed bands is still under debate. PL spectra of SnO_2 and FTO typically present four emission bands in which the less energetic one (centered near ~500 nm or 2.5 eV) has been associated to electron transitions mediated by oxygen vacancies levels in the band gap. Alternatively, Trani et al. [45] ascribed this band in SnO_2 to the appearance of a fully occupied flat energy level lying at about 1 eV above the valence band and an empty level resonant with the conduction band. Moreover, based on positron annihilation experiments, Zhou et al. [46] have supported the origin of this 2.5 eV band as electron transitions from a V_O^+ energy hybridized with the conduction band to a V_O^{2+} energy level.

Instead of the typically used UV excitation, we have recorded PL spectra by using visible light (at 488 nm, below the band gap) to study in detail the 2.5 eV (around 500 nm) emission band. Fig. 8 presents the PL spectra for the three series evidencing that H_2 addition in the

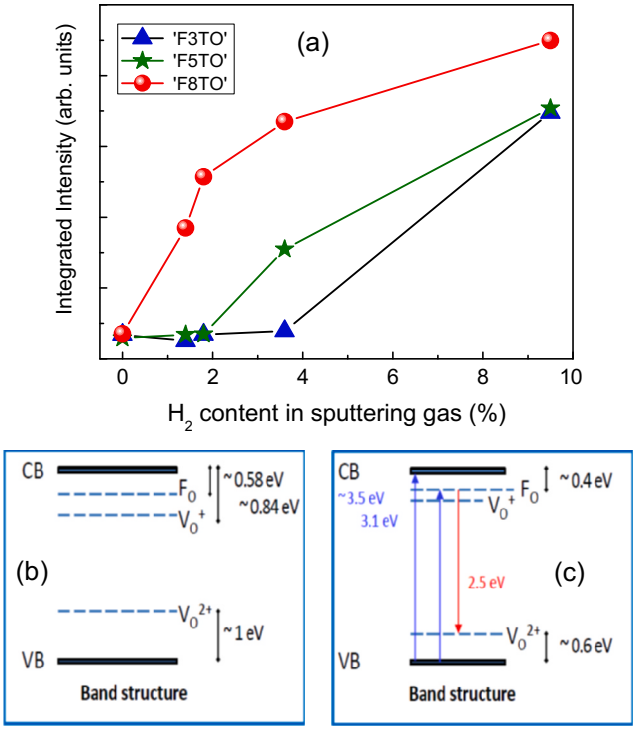

Fig. 9. (a) Evolution of the integrated area intensity of photoluminescence in studied series. (b) Energy levels in SnO_2, (c) Energy levels in FTO.

sputtering gas increases the PL intensity of the 502 nm band. It should be noted that the wavelength range in which this PL band appears coincides with the characteristic Raman spectrum of SnO_2 using 488 nm exciting wavelength; however, the very low Raman signal does not perturb significantly the PL band. Fig. 9 shows that H_2 promotes more efficiently the PL emission at 502 nm as the nominal fluorine content is increased. In the assumption that this PL band is related to oxygen vacancy energy levels in the gap, its intensity accounts for the density of oxygen defects. The results in Figs. 8 and 9 evidence that, independently of the fluorine content, the samples prepared without H_2 have very low amount of oxygen vacancy defects and that defects are generated more efficiently in series with higher fluorine content. For example, 'F8TO' reaches a similar defect densitiy in samples deposited with ~4% H_2 as those obtained with 9.5% H_2 in 'F5TO' and 'F3TO' series.

In order to explain the effect of H_2 on the electronic structure of FTO, we have considered the reported SnO_2 and FTO band structures [46] in which fluorine incorporation at oxygen site (F_O) slightly shifts the energy levels of oxygen vacancies V_O^{2+} and V_O^{+} towards the band edges (Fig. 9(c)) compared to SnO_2 (Fig. 9(b)). This scheme let us identify the absorption and emission features observed in our samples (Fig. 9(c)). The energy gap ranges from 3.63 to 3.40 eV (represented as ~3.5 eV in Fig. 9(b)) for samples prepared without H_2, as shown in Fig. 4.

Additionally, the intensity of the broad absorption band at 400 nm (~3.1 eV) (Fig. 3 and Ref. [19]) depends both on fluorine and H_2 gas content. Its dependence on the fluorine content indicates that the transition has to be related to fluorine at oxygen vacancies (F_O) and corresponds to transitions from the VB to F_O energy levels (Fig. 9(c)). The monotonous dependence of this broad band with H_2 (Fig. 3) should be related with changes in the VB due to the monotonous partial reduction of Sn^{4+} to Sn^{2+} observed in XAS experiments.

On the other hand, the intensity of the 2.5 eV (502 nm) PL emission band also depends on both the fluorine content and the H_2 gas amount, indicating that this band is related to transitions from F_O to V_O^{2+} energy levels. The dependence on H_2 is due to generation of oxygen vacancies by Sn^{2+} in the SnO_2 mother structure. This explanation is in agreement with the reported band structure in [46] and explains small variations of energy level values as shown in Fig. 9(c), giving F_O energy levels at ~0.4 eV below the CB and V_O^{2+} energy level at ~0.6 eV above the VB.

4. Discussion

To summarize the observed behaviors vs. the H_2 content in sputtering gas along the studied series we can consider the following facts: (i) there is no dependence on H_2 of the film atomic composition (including H); (ii) the use of H_2 in the sputtering gas improves the electrical conductivity up to saturation in 'F3TO' and 'F5TO' series and presents maximal values for ~4% H_2 content in 'F8TO'; (iii) high transparency is obtained in all samples up to 4% H2 and a broad absorption band around 400 nm is clearly observed in samples with high H_2 content, (iv) in 'F3TO' and 'F5TO'series band gap energy decreases while in 'F8TO' the gap presents maximal values for 4–6% H_2; (v) F content in the films and H_2 in the sputtering gas favor film amorphization; (vi) a small but continuous decrease of Sn oxidation state is observed vs. H_2 content in sputtering gas; (vii) oxygen defects are generated by using H_2 being more effective in high fluorine content series.

The many techniques used in this study allow the understanding of apparently contradictory results regarding the constant actual content of hydrogen in the films but their radically different optical and electrical properties. Increasing H_2 content in the sputtering gas, does not increase hydrogen concentration in the films but reduces the average oxidation state of Sn^{4+} (observed by XAS) by inducing the formation of Sn^{2+} and oxygen vacancies that decrease long-range order and finally leads to amorphous films. These oxygen vacancies modify the optical transmission and PL spectra by providing shallow in-gap defect-states (substitutional F and O vacancies) and explain the improvement of conductivity by the generation of charge carriers.

The resistivity behavior is rather complex but some clear correlations can be highlighted. An increase in conductivity is clearly observed in series with low fluorine content (up to 5%) which is found to saturate in coincidence with crystallinity hindering (Figs. 2 and 5). On the other hand, the amorphous character shown by the 'F8TO' series is key to explain its electrical behavior as the competition between the generation of charge carriers and amorphization. In high fluorine content samples ('F8TO' series) the joint effect of oxygen substitution by fluorine ions (F_O) and the excess of oxygen vacancies (V_O^{2+} and V_O^{+} provided by H_2) is detrimental for the long-range order, that is a typical cause of conductivity worsening in TCMs. Consequently, series with moderately high fluorine content (> 5%) and enough Sn^{2+} amount (due to H_2 gas) become amorphous hampering generation of charge carriers in the CB and decreasing charge mobility. Conversely, series with low fluorine content (< 5%) present an increase of charge carrier density that improves conductivity up to saturation (within the studied range) due to amorphization.

5. Conclusions

The effect of using H_2 in sputtering gas to prepare FTO films at room temperature from SnO_2-SnF_2 cathodes with several fluorine contents has been studied. From the macroscopic point of view, conductivity has a complex behavior depending on fluorine content in the film and H_2 concentration in sputtering gas, but high transparence at visible wavelengths is obtained for all samples. The variation of fluorine doping and the H_2 content in sputtering gas allows improvements of four orders of magnitude in film conductivity.

Microscopic characterizations let us conclude that H_2 in sputtering gas causes a slight reduction of Sn^{4+} in FTO films that consequently creates oxygen vacancies and promotes amorphization. The competition between reduction of Sn^{4+} and amorphization explains the

complex behavior of electric transport properties. Optimized F doping and H_2 gas content can deliver excellent values of sheet resistance (20 Ω/□) with optical transmission (> 90%) for films grown at room temperature on fused silica as well as on flexible substrates (PET).

CRediT authorship contribution statement

María Morán-Pedroso: Investigation, Resources. **Raúl Gago:** Investigation, Writing - original draft. **Jaakko Julin:** Investigation, Resources. **Eduardo Salas-Colera:** Investigation, Resources. **Ignacio Jimenez:** Investigation. **Alicia de Andrés:** Methodology, Writing - review & editing. **Carlos Prieto:** Conceptualization, Methodology, Writing - original draft.

Declaration of Competing Interest

The authors declare that they have no known competing financial interests or personal relationships that could have appeared to influence the work reported in this paper.

Acknowledgements

This research has received funding from grants RTI2018-096918-B-C41 and RTI2018-095137-B-I00 of the Ministerio de Ciencia e Innovación (Spain) and from PIE201660E016 of CSIC. We thank HZB and HZDR for the allocation of beamtime for synchrotron and ion beam analysis experiments, respectively. The access to BESSY-II has been granted through agreement n° 226716 from the European Community's Seventh Framework Programme (FP7/2007-2013). Finally, the technical assistance from R. Abrudan at BESSY-II is also greatly appreciated.

Appendix A. Supplementary material

Supplementary data to this article can be found online at https://doi.org/10.1016/j.apsusc.2020.147906.

References

[1] H.L. Hartnagel, A.L. Dawar, A.K. Jain, C. Jadadish, Semiconducting Transparent Thin Films, Institute of Physics, Bristol, 1995.
[2] K. Ellmer, R. Mientus, S. Seeger, Metallic Oxides (ITO,ZnO, SnO2, TiO2), in: D. Levy, E. Castellon (eds.), Transparent Conductive Materials: Materials Synthesis, Characterization, Applications, Wiley-VCH Verlag GmbH & Co. KGaA, Weinheim, 2018.
[3] T. Minami, New n-type transparent conducting oxides, MRS Bull. 25 (2000) 38.
[4] A.N. Benerjee, K.K. Chattopadhyay, Recent developments in the emerging field of crystalline p-type transparent conducting oxide thin films, Prog. Cryst. Growth Charact. Mater. 50 (2005) 52–105.
[5] M. Ait Aouaj, R. Diaz, A. Belayachi, F. Rueda, M. Abd-Lefdil, Comparative study of ITO and FTO thin films grown by spray pyrolysis, Mat. Res. Bull. 44 (2009) 1458–1461.
[6] A.C. Arias, L.S. Roman, T. Bugler, R. Toniolo, M.S. Meruvia, I.A. Hummelgen, The use of tin oxide thin films as a transparent electrode in PPV based light-emitting diodes, Thin Solid Films 371 (2000) 201–206.
[7] H. Kim, R.C.Y. Auyeung, A. Piqué, Transparent conducting F-doped SnO2 thin films grown by pulsed laser deposition, Thin Solid Films 516 (2008) 5052–5056.
[8] Y. Zhou, W. Xu, J. Li, Ch. Yin, Y. Liu, B. Zhao, Z. Chen, Ch. He, W. Mao, K. Ito, Vacancy defects and optoelectrical properties for fluorine tin oxide thin films with various SnF2 contents, J. Appl. Phys. 123 (2018) 025706-1–025706-8.
[9] S.-T. Zhang, J.L. Rouvière, V. Consonni, H. Roussel, L. Rapenne, E. Pernot, D. Muñoz-Rojas, A. Klein, D. Bellet, High quality epitaxial fluorine-doped SnO2 films by ultrasonic spray pyrolysis: structural and physical property investigation, Mater. Des. 132 (2017) 518–525.
[10] T. Jäger, Y.E. Romanyuk, A.N. Tiwari, A. Anders, Controlling ion fluxes during reactive sputter-deposition of SnO_2:F, J. Appl. Phys. 116 (2014) 033301-1–033301-7.
[11] Z.Y. Banyamin, P.J. Kelly, G. West, J. Boardman, Electrical and optical properties of fluorine doped tin oxide thin films prepared by magnetron sputtering, Coatings 4 (2014) 732–746.
[12] F. Wu, X. Tong, Z. Zhao, J. Gao, Y. Zhou, P. Kelly, Oxygen-controlled structures and properties of transparent conductive SnO_2: F films, J. Alloy Compd. 695 (2017) 765–770.
[13] S. Yu, L. Li, X. Lyu, W. Zhang, Preparation and investigation of nano-thick FTO/Ag/FTO multilayer transparent electrodes with high figure of merit, Sci. Rep.-UK 6 (2016) 20399, https://doi.org/10.1038/srep20399.
[14] B.L. Zhu, X. Zhao, W.C. Hu, T.T. Li, J. Wu, Z.H. Gan, J. Liu, D.W. Zeng, C.S. Xie, Structural, electrical, and optical properties of F-doped SnO or SnO_2 films prepared by RF reactive magnetron sputtering at different substrate temperatures and O_2 fluxes, J. Alloy Compd. 719 (2017) 429–437.
[15] B.L. Zhu, F. Liu, K. Li, K. Lv, J. Wu, Z.H. Gan, J. Liu, D.W. Zeng, C.S. Xie, Sputtering deposition of transparent conductive F-doped SnO_2 (FTO) thin films in hydrogen-containing atmosphere, Ceram. Int. 43 (2017) 10288–10298.
[16] S. Ishibashi, Y. Higuchi, Y. Ota, K. Nakamura, Low resistivity indium–tin oxide transparent conductive films. I. effect of introducing H_2O gas or H_2 gas during direct current magnetron sputtering, J. Vac. Sci. Technol. A 8 (1990) 1399–1402.
[17] K. Zhang, F. Zhu, C.H.A. Huan, A.T.S. Wee, Indium tin oxide films prepared by radio frequency magnetron sputtering method at a low processing temperature, Thin Solid Films 376 (2000) 255–263.
[18] L. Álvarez-Fraga, F. Jiménez-Villacorta, J. Sánchez Marcos, A. de Andrés, C. Prieto, Room temperature preparation of indium-tin oxide thin films on transparent flexible substrates, Appl. Surf. Sci. 344 (2015) 217–222.
[19] M. Morán-Pedroso, J. Sánchez Marcos, A. de Andrés, C. Prieto, Fluorinated tin oxide (FTO) deposited at room temperature: influence of hydrogen and oxygen in the sputtering gas on the optical and electrical properties, Appl. Surf. Sci. 459 (2018) 349–353, https://doi.org/10.1016/j.apsusc.2018.08.011.
[20] L.J. van der Pauw, A method of measuring specific resistivity and Hall effect of discs of arbitrary shape, Philips Res. Rep. 13 (1958) 1–9.
[21] L.J. van der Pauw, A method of measuring the resistivity and hall coefficient on lamellae of arbitrary shape, Philips Tech. Rev. 20 (1958) 220–224.
[22] G.E. Jellison, V.I. Merkulov, A.A. Puretzky, D.B. Geohegan, G. Eres, D.H. Lowndes, J.B. Caughman, Characterization of thin-film amorphous semiconductors using spectroscopic ellipsometry, Thin Solid Films 377–378 (2000) 68–73.
[23] A. Climent-Font, F. Pászti, G. García, M.T. Fernández-Jiménez, F. Agulló, First measurements with the Madrid 5 MV tandem accelerator, Nucl. Instrum. Meth. B 219–220 (2004) 400–404.
[24] N.P. Barradas, C. Jeynes, R.P. Webb, Simulated annealing analysis of Rutherford backscattering data, Appl. Phys. Lett. 71 (1997) 291–293.
[25] N.P. Barradas, C. Jeynes, Advanced physics and algorithms in the IBA Data Furnace, Nucl. Instrum. Meth. B 266 (2008) 1875–1879.
[26] M.C. Choi, Y. Kim, C.S. Ha, Polymers for flexible displays: from material selection to device applications, Prog. Polym. Sci. 33 (2008) 581630.
[27] A. Iwan, I. Tazbir, M. Sibiński, B. Boharewicz, G. Pasciak, E. Schab-Balcerzak, Optical, electrical and mechanical properties of indium tin oxide on polyethylene terephthalate substrates: application in bulk-heterojunction polymer solar cells, Mater. Sci. Semicond. Process. 24 (2014) 110–116.
[28] M.H. Ahn, E.S. Cho, S.J. Kwon, Characteristics of ITO-resistive touch film deposited on a PET substrate by in-line DC magnetron sputtering, Vacuum 101 (2014) 221–227.
[29] M. Acosta, J. Mendez-Gamboa, I. Riech, C. Acosta, M. Zambrano, AZO/Ag/AZO multilayers electrodes evaluated using a photonic flux density figure of merit for solar cells applications, Superlattice. Microst. 127 (2019) 49–53.
[30] A.K. Akhmedov, A.K. Abduev, V.M. Kanevsky, A.E. Muslimov, A.S. Asvarov, Low-temperature fabrication of high-performance and stable GZO/Ag/GZO multilayer structures for transparent electrode applications, Coatings 10 (2020) 269.
[31] Y. Demirhan, H. Koseoglu, F. Turkoglu, Z. Uyanik, M. Ozdemir, G. Aygun, L. Ozyuzer, The controllable deposition of large area roll-to-roll sputtered ITO thin films for photovoltaic applications, Renew. Energ. 146 (2020) 1549–1559.
[32] J. Tauc, Amorphous and Liquid Semiconductors, Plenum, London, 1974.
[33] A.R. Zanatta, Revisiting the optical bandgap of semiconductors and the proposal of a unified methodology to its determination, Sci. Rep. 9 (2019) 11225.
[34] Ł. Jarosiński, J. Pawlak, S.K.J. Al-Ani, Inverse logarithmic derivative method for determining the energy gap and the type of electron transitions as an alternative to the Tauc method, Opt. Mater. 88 (2019) 667–673.
[35] N. Haddad, Z. Ben Ayadi, H. Mahdhi, K. Djessas, Influence of fluorine doping on the microstructure, optical and electrical properties of SnO_2 nanoparticles, J. Mater. Sci. Mater. Electron. 28 (2017) 15457–15465.
[36] C. McGuinness, C.B. Stagarescu, P.J. Ryan, J.E. Downes, D. Fu, K.E. Smith, R.G. Egdell, Influence of shallow core-level hybridization on the electronic structure of post-transition-metal oxides studied using soft X-ray emission and absorption, Phys. Rev. B 68 (2003) 165104.
[37] J.A. McLeod, N.A. Skorikov, L.D. Finkelstein, E.Z. Kurmaev, A. Moewes, Chemical bonding and hybridization in 5p binary oxide, J. Phys. Chem. C 116 (2012) 24248–24254.
[38] Dong-won Choi, W.J. Maeng, Jin-Seong Park, The conducting tin oxide thin films deposited via atomic layer deposition using Tetrakis-dimethylamino tin and peroxide for transparent flexible electronics, Appl. Surf. Sci. 313 (2014) 585–590.
[39] C.S. Yeo, K.B. Chung, J.S. Park, J.H. Song, Enhancement of the Hall mobility in-hydrogen-ion-irradiated ZnO Films, J. Korean Phys. Soc. 60 (2012) 307–310.
[40] M.S. Moreno, R.F. Egerton, P.A. Midgley, Differentiation of tin oxides using electron energy-loss spectroscopy, Phys. Rev. B 69 (2004) 233304.
[41] M. Gaidi, A. Hajjaji, R. Smirani, B. Bessais, M.A. El Khakani, Structure and photoluminescence of ultrathin films of SnO_2 nanoparticles synthesized by means of pulsed laser deposition, J. Appl. Phys. 108 (2010) 063537.
[42] F. Gu, S.F. Wang, C.F. Song, M.K. Lü, Y.X. Qi, G.J. Zhou, D. Xu, D.R. Yuan, Chem. Phys. Lett. 372 (2003) 451–454.
[43] Y. Sakurai, Photoluminescence of oxygen-deficient-type defects in γ-irradiated silica glass, J. Non-Cryst. Solids 352 (2006) 5391–5398.
[44] J.X. Zhou, M.S. Zhang, J.M. Hong, Z. Yin, Raman spectroscopic and photoluminescence study of single-crystalline SnO2 nanowires, Solid State Commun. 138 (2006) 242–246.
[45] F. Trani, M. Causa, D. Ninno, G. Cantele, V. Barone, Density functional study of oxygen vacancies at the SnO_2 surface and subsurface sites, Phys. Rev. B 77 (2008) 245410.
[46] Y. Zhou, W. Xu, J. Li, C. Yin, Y. Liu, B. Zhao, Z. Chen, C. He, W. Mao, K. Ito, Vacancy defects and optoelectrical properties for fluorine tin oxide thin films with various SnF2 contents, J. Appl. Phys. 123 (2018) 025706.